Hindawi
Journal of Nanomaterials
Volume 2019, Article ID 6090259, 12 pages
https://doi.org/10.1155/2019/6090259

Research Article

Size-Dependent Cytotoxicity and Genotoxicity of Silver Nanoparticles in Cochlear Cells *In Vitro*

Maria Perde-Schrepler,[1] **Adrian Florea**,[2] **Ioana Brie**,[1] **Piroska Virag**,[1] **Eva Fischer-Fodor**,[1] **Angela Vâlcan**,[3] **Eugen Gurzău**,[3] **Cosmin Lisencu**,[4] **and Alma Maniu**[5]

[1]*Department of Radiobiology and Tumor Biology, Oncology Institute "Prof. Dr. Ion Chiricuță", 34-36 Republicii Street, 400015 Cluj-Napoca, Romania*
[2]*Department of Cell and Molecular Biology, Faculty of Medicine, "Iuliu Hațieganu" University of Medicine and Pharmacy, 6 Louis Pasteur Street, 400349 Cluj-Napoca, Romania*
[3]*Environmental Health Center, 58 Busuiocului Street, 400240 Cluj-Napoca, Romania*
[4]*Department of Oncologic Surgery, "Iuliu Hațieganu" University of Medicine and Pharmacy, 34-36 Republicii Street, 400015 Cluj-Napoca, Romania*
[5]*Department of Otolaryngology-Head and Neck Surgery, "Iuliu Hațieganu" University of Medicine and Pharmacy, 4-6 Clinicilor Street, 400006 Cluj-Napoca, Romania*

Correspondence should be addressed to Adrian Florea; aflorea@umfcluj.ro

Received 28 September 2018; Accepted 29 November 2018; Published 26 February 2019

Academic Editor: Dong Kee Yi

Silver nanoparticles (AgNPs) have been proven to have potent antibacterial properties, offering an attractive alternative to antibiotics in the treatment of several infections such as otitis media. Concerns have been raised though regarding their toxicity. There are few data regarding the toxic effects of AgNPs in cochlear cells. The aim of our study was to evaluate the effects of AgNPs of four sizes as a function of their size on HEI-OC1 cochlear cells and on HaCaT keratinocytes. The cells were treated with different concentrations of AgNPs. We evaluated silver uptake by atomic absorption spectroscopy and transmission electron microscopy (TEM), cytotoxicity with the alamarBlue test, ROS production with 2′,7′-dichloro-dihydro-fluorescein diacetate, and genotoxicity with the comet assay. Silver intracellular concentration increased proportionally with the incubation time and the size of the NPs. Silver uptake was higher in HEI-OC1 cells compared to HaCaT. While after 4 h exposure, only the 50 nm NPs were observed in both cell lines and only the 5 nm NPs were observed in the HaCaT cells, after 24 h, nanoparticles of all sizes could be visualized in both cell lines. The cells showed signs of distress: vacuolizations, autophagosomes, signs of apoptosis, or cellular debris. AgNPs of all sizes reduced viability proportionally with the concentration, HEI-OC1 cells being more affected. The toxicity of AgNPs decreased with the nanoparticle size, and ROS production was dose and size dependent, mainly in the cochlear cells. Genotoxicity assessed by comet assay revealed a higher level of DNA lesions in HEI-OC1 cells after treatment with small-sized AgNPs. The perspective of using AgNPs in the treatment of otitis media, although very attractive, must be regarded with caution: cochlear cells proved to be more sensitive to the toxic effect of AgNPs compared to other cell lines. Potential treatments must be tailored specifically, choosing NPs with minimum toxicity towards auditory cells.

1. Introduction

Chronic otitis media is a significant public health problem affecting 0.5–30% of the population, with severe complications such as sensorineural hearing loss [1] and vestibular impairment [2]. Treatment with antibiotics is hampered by the appearance of multidrug resistant strains of bacteria as well as the formation of bacterial biofilm in the middle ear of patients with chronic otitis media [3]. Having different mechanisms of action, AgNPs could overcome the

disadvantages of antibiotic therapy as was shown in a clinical study using a preparation containing AgNPs and obtaining the elimination of clinical symptoms, the reduction of pathological exudation, and stimulation of the epidermization process during 6 months of observation time [4]. There are still questions regarding the mechanisms by which AgNPs exert their antimicrobial effect. AgNPs can penetrate the bacterial cell wall causing a structural change of the cell membrane and an increase in cell permeability, both of which leads to cell death. The formation of free radicals and subsequent free radical-induced membrane damage is another mechanism. It has also been found that AgNPs can release silver ions and interact with the thiol groups of many vital enzymes and phosphorus-containing bases, thus inhibiting cell division and DNA replication [5]. In the years to come, the number of applications using the antimicrobial properties of AgNPs are likely to further increase, thus the assessment of the risks AgNPs represent for the mammalian cells must be a priority [6]. At ear level, AgNPs are able to pass through the round and oval windows after transtympanic injection reaching the structures of the inner ear as shown by microCT in a study conducted by Zou et al. [7].

Several studies demonstrated the cytotoxicity of AgNPs towards different types of cells, such as human peripheral blood mononuclear cells [8], lung epithelial cells [9], neuroendocrine cells [10], macrophages, stem cells [11, 12], osteoblasts [13], and many others, interfering with their cellular functions and causing DNA damage and apoptosis. Regarding the mechanisms of these toxic effects, the influence of AgNPs on the formation of free radicals is mentioned [14]. According to numerous reports, the overproduction of free radicals, which leads to oxidative stress, is caused by ions being released from silver nanoparticles, including by a Trojan horse-type mechanism [15]. The size of the nanoparticles is considered to be one of the most important factors influencing their toxicity [16].

Having these in mind, our study is aimed at assessing the potential risk of using AgNPs in the middle and inner ear, evaluating their uptake in the cochlear cells and their toxicity as a function of size.

2. Material and Methods

2.1. Cell Lines and Culture. The first line of cells used in this study was the spontaneously immortalized human keratinocyte cell line HaCaT. These cells were purchased from the Cell Line Service of the German Cancer Research Centre in Heidelberg and maintained in high glucose Dulbecco's Modified Eagles' Medium (DMEM) supplemented with 10% heat-inactivated FBS, 2 mM glutamine, 50 UI/ml penicillin, and 50 mg/ml streptomycin (all media were from Sigma-Aldrich Chemie GmbH, Taufkirchen, Germany).

The second cell line used by us (and of particular interest) was the HEI-OC1 cell line, a gift from Prof. Federico Kalinek from the House Ear Institute (Los Angeles, USA). It was developed from the inner ear hair cells of the transgenic "Immortomouse." The cells were cultured under permissive conditions (33°C, 10% CO_2) in high glucose DMEM supplemented with 10% bovine fetal serum (FBS).

2.2. Silver Nanoparticles. Polyvinylpyrrolidone- (PVP-) coated silver nanoparticles (Table 1) were purchased from nanoComposix (San Diego, CA, USA) in four sizes and were characterized by the manufacturer regarding their diameter, surface area, mass concentration, particle concentration, hydrodynamic diameter, zeta potential, pH, and maximum absorption (optical density).

2.2.1. Characterization of AgNPs by Transmission Electron Microscopy (TEM). 5 μl from each AgNP suspension were pipetted on 300 mesh formvar- (Electron Microscopy Sciences, Hatfield, PA, USA) coated Cu grids (Agar Scientific Ltd., Stansted, UK). After 5 min, the excess suspension was removed with filter paper. The samples were examined on a JEOL JEM-1010 transmission electron microscope operating at 80 kV acceleration voltage and photographed with a MegaView III camera (Olympus, Soft Imaging System, Münster, Germany).

2.3. Atomic Absorption Spectroscopy for the Silver Uptake. The cells were seeded on 6-well plates at a density of 5×10^5 cells/well and separately treated with 50 μg/ml of AgNPs of each size. After 4 h and 24 h of incubation, the cells were trypsinized, counted, washed, and centrifuged. The cellular pellets were placed in a −80°C freezer until they were processed for the evaluation of silver uptake. The samples were treated with 100 μl of HNO_3 65% (Merck KGaA, Darmstadt, Germany), vortexed, and placed in an incubator for 48 h at 37°C. After mineralization, the samples were diluted in 1 ml ultrapure water and analyzed on a ZEEnit 700 P atomic absorption spectrophotometer (Analytik Jena AG, Jena, Germany) using the electrothermic atomization technique in a graphite oven (GFAAS; ETAAS). The samples were analyzed by the standard addition method.

2.4. TEM for AgNP Cellular Uptake. HEI-OC1 and HaCaT cells from both the control groups and the cells exposed to 50 μg/ml of AgNPs of the four sizes, incubated for 4 h and 24 h, respectively, were processed for TEM. They were fixed for 1.5 h with 2.7% glutaraldehyde (Electron Microscopy Sciences, Hatfield, PA, USA) in 0.1 M phosphate buffer (pH 7.4), washed four times with the same buffer, and post-fixed for 1.5 h with 1.5% osmium tetroxide (Sigma-Aldrich, St. Louis, USA) in 0.15 M phosphate buffer (pH 7.4). The cells were dehydrated in an ethanol series and embedded in EMBed 812 resin (Electron Microscopy Sciences, Hatfield, PA, USA). Fixation and the first several steps of dehydration were performed at 4°C and the resin was polymerized at 60°C for 72 h. Ultrathin sections of 60–80 nm were cut with a DiATOME diamond knife (DiATOME, Hatfield, PA, USA) on a LKB Ultrotome 8800 III Bromma ultramicrotome (LKB Produckter AB, Stockholm-Bromma, Sweden). The sections collected on 300 mesh formvar-coated Cu grids (Agar Scientific Ltd., Stansted, UK) were contrasted for only 7 min with a saturated solution of uranyl acetate (Merck, Billerica, USA) for a better visualization of the NP distribution within the cells. The samples were examined on a JEOL JEM-1010 transmission electron microscope operating at 80 kV acceleration voltage and photographed with a

Table 1: PVP-coated AgNPs from NanoComposix—characteristics offered by the manufacturer.

Parameter	5 nm	25 nm	50 nm	110 nm
Diameter (TEM) (nm)	6.3 ± 1.4	21.2 ± 7.9	51 ± 9	110 ± 14
Surface area (m^2/g)	82.1 (TEM)	21.3 (TEM)	10.7 (calculated)	5.1 (calculated)
Mass concentration (Ag) (mg/ml)	5.03	5.2	5.35	5.19
Particle concentration (particles/ml)	$3.6E+15$	$1.0E+14$	$1.3E+08$	$7.2E+11$
Hydrodynamic diameter (nm)	Not reported	41.5	86	136
Zeta potential (mV)	Not reported	−40.4	−55	−32
Particle surface	PVP	PVP	PVP	PVP 40 kDa (polymer)
pH of solution	5.8	5.2	4.6	4.8
λ max (nm)	405	399	430	509
MaxOD	623.04	757.98	582.68	189.33
Solvent	Milli-Q water	Milli-Q water	Milli-Q water	Milli-Q water

MegaView III camera (Olympus, Soft Imaging System, Münster, Germany).

2.5. Cytotoxicity of the Silver Nanoparticles. The viability of the cells after exposure to AgNPs was assessed with the alamarBlue fluorimetric test (Molecular Probes, Invitrogen, Carlsbad, CA, USA). Resazurin, the active ingredient in alamarBlue reagent, is a nontoxic, cell permeable compound, blue and virtually nonfluorescent. Upon entering the cells, resazurin is reduced to resofurin, a red, highly fluorescent compound. Viable cells continuously convert resazurin to resofurin, increasing fluorescence in time. The cells were plated in 96-well plates (Nunc, Thermo Scientific, Waltham, MA, USA) at a density of 2×10^4 cells/well. Treatments were done with serial dilutions of the AgNPs of four sizes (5, 25, 50, and 110 nm). For HEI-OC1 cells, the following concentrations were used: 100, 50, 35, 20, 10, 5, 2.5, 1, 0.5, 0.25, and 0.1 μg/ml. For HaCaT cells, four additional concentrations were used in order to obtain 100% inhibition of viability: 250, 500, 750, and 1000 μg/ml. For each experiment, cells from at least three wells were left untreated (control). After 24 h incubation, the cells were treated with 20 μl/well of alamarBlue Reagent and incubated in standard cell culture conditions for 1 h. The emitted fluorescence was read on a BioTek Synergy 2 microplate reader at 570 nm excitation and 585 nm emission. At each concentration, the surviving fraction was calculated as fluorescence of the sample/fluorescence of control (nontreated cells) × 100. Each experiment was repeated 3 times. 50% inhibitory concentration (IC50), the concentration of the compound which reduced viability by 50%, was calculated using nonlinear regression and four-parameter sigmoid curves.

2.6. Generation of Reactive Oxygen Species (ROS). HEI-OC1 and HaCaT cells were treated with AgNPs as follows: 5 and 10 μg/ml for HEI-OC1 cells and 50 and 100 μg/ml for HaCaT; these concentrations were chosen according to the average IC50 of NPs on the two cell lines. After 2 h and 4 h of incubation, the cells were washed with PBS and labelled with 1 μg/ml of 2′,7′-dichlorofluorescein diacetate (DCFDA) (Molecular Probes, Invitrogen, Carlsbad, CA, USA) for 30 min. The emitted fluorescence was recorded with a BioTek Synergy 2 microplate reader (BioTek Instruments Inc., Winooski, VT, USA) at 495 nm excitation and 529 nm emission.

2.7. Comet Assay. The effect of AgNPs on the DNA of HEI-OC1 and HaCaT cells was evaluated with the alkaline single cell gel electrophoresis assay or Comet assay, according to a protocol presented elsewhere [17]. Briefly, the cells were treated with 50 μg/ml AgNPs. After 2 h and 4 h of incubation, the cells were trypsinized, washed, and included in 1% low melting point agarose at a density of 10^6 cells/ml. This suspension was layered onto microscope slides pretreated with normal melting point agarose. The slides were placed in Coplin jars in a lysis solution at 4°C for 24 h. After this interval, the slides were placed in a horizontal electrophoresis tank in an alkaline (pH > 13) electrophoresis solution for 20 min for DNA unwinding. A uniform electric field of 1 V/cm was then applied for 20 min. After neutralization and fixation, the slides were stained with ethidium bromide and analyzed at a fluorescence microscope (Zeiss, Germany—excitation 510–560 nm, detection 590 nm) with an objective of 40× magnification. The DNA migrated in an electric field depending on the amount and severity of the lesions resulting in a comet-like aspect. The comets were classified into 5 classes: 0, intact DNA, no tail; 1–4, comets with increasing length tails (Figure 1). 200 cells/sample were analysed and a lesion score (LS) was calculated with the following formula:

$$\mathrm{LS[AU]} = \frac{\sum[(\text{no. of cells in class } x) \bullet (x)]/\text{no. of cells}}{100}, \quad (1)$$

where x is the number of the class a cell is attributed to: 0, 1, 2, 3, or 4.

3. Results

3.1. Characterization of AgNPs by TEM. The aspect, size, and distribution of AgNPs are presented in Figure 2. Most of the AgNPs were dispersed relatively uniformly in the solution and were round in shape (Figures 2(b)–2(d)); however, mainly among the 110 nm NPs, triangular, pentagonal,

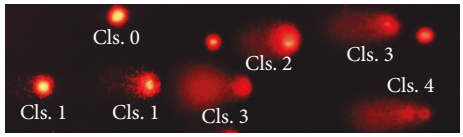

Figure 1: Microscopic aspect of cellular DNA after migration in an electric field with ethidium bromide staining. Magnification 40x. Cls. 0–4: different classes of comets, according to their tail lengths.

hexagonal, and rare octagonal NPs were found (Figure 2(d)). The 5 nm NPs appeared grouped in small clusters occupying the entire surface of the grid (Figure 2(a)). The TEM images of the coated AgNPs dispersed in water confirmed the primary particle size stated by the manufacturers.

3.2. AgNP Uptake: Atomic Absorption Spectroscopy. After treatment for 4 h and 24 h, respectively, with 50 μg/ml of the four types of AgNPs, the intracellular silver concentration was assessed by atomic absorption spectroscopy. Silver concentration in the HEI-OC1 cells and HaCaT cells increased proportionally with the incubation time (Figures 3(a) and 3(b)).

After 4 h incubation time, the HaCaT cell line had slightly higher concentrations of intracellular silver compared to HEI-OC1 cells for all the NPs but this difference was not significant (Figure 3(a)). After 24 h, the silver concentration was higher in the HEI-OC1 cells, the difference being significant for the 50 nm NPs ($p < 0.5$, two-way ANOVA, Bonferroni posttest) (Figure 3(b)). At 24 h, the intracellular silver concentration increased proportionally with the NP sizes in both cell lines (Figure 3(b) and Table 2).

3.3. AgNP Uptake: TEM

3.3.1. Control Cells. Control HaCaT cells (Figure 4(a)) showed indented euchromatic nuclei, with prominent nucleoli, cell organelles (especially mitochondria and rough endoplasmic reticulum), and important amounts of glycogen. In these cells, the plasma membrane displayed a high number of extracellular extensions, often branched. Control HEI-OC1 cells (Figure 4(b)) contained large, oval-round, predominantly euchromatic nuclei, with 1-2 nucleoli. Their cytoplasm presented many free ribosomes and a few short profiles of rough endoplasmic reticulum, and the plasma membrane exhibited a low number of short and thin extensions.

3.3.2. Cells Treated with AgNps

(1) HaCaT Cells. TEM examination of the HaCaT cells incubated with the AgNPs in the different experimental conditions showed a high ability of these cells to accumulate NPs (Figure 5). Thus, after 4 h incubation with the 5 nm AgNPs, the NPs were found in endosomes, in the cytosol, and inside lysosomes (not shown). We also found cellular debris with attached NPs (not shown). After 24 h incubation, the AgNPs were found in the HaCaT cells in extremely large endosomes (inset of Figure 5(a)), in the cytosol (not shown), and inside the lysosomes (Figure 5(a)). The 5 nm AgNPs were still aggregated in clusters, a phenomenon that facilitated their identification. The cells also contained many cytoplasmic vacuoles and a reduced number of plasma membrane extensions (Figure 5(a)). No AgNPs were found in the HaCaT cells incubated for 4 h with the 25 nm AgNPs, but an increased number of autophagosomes were observed (not shown). After 24 h incubation, the 25 nm AgNPs were rarely found in endosomes (not shown) and dispersed into the cytoplasm (Figure 5(b)), and many lysosomes containing NPs were observed in almost all the examined cells (Figure 5(b)). Autophagosomes in increased number were found, as well as many apoptotic cells (not shown).

Consecutive to the 4 h incubation with the 50 nm AgNPs, some HaCaT cells contained the NPs in endosomes (not shown). Many cells containing large numbers of autophagosomes were also observed (not shown). The 24 h incubation with the 50 nm AgNps resulted in the highest amount of NPs captured in the cells in our study; they were rarely visible while they were still packed in endosomes (not shown) or grouped in small clusters inside the cytosol (Figure 5(c)). Most of the examined cells contained a high number of lysosomes with NPs (Figure 5(c)). The cells displayed a lower number of extensions as compared to the control cells (Figure 5(c)), and a low number of dead cells were noted (not shown). After 4 h incubation of the HaCaT cells with the 110 nm AgNPs, we could not find on the examined sections the NPs inside the cells (not shown). However, among the cells with normal ultrastructural features, many cells exhibited cytoplasmic vacuolation and a high number of autophagosomes, while some cells were dead (not shown). Consecutive to the 24 h incubation, the 110 nm AgNPs were captured by the HaCaT cells in high number inside the endosomes or free in the cytosol—more or less grouped in clusters—and inside many lysosomes (Figure 5(d)). Most of the examined cells showed only a few plasma membrane extensions (Figure 5(d)).

(2) HEI-OC1 Cells. The cells in this line showed a much lower ability to accumulate AgNPs as compared to HaCaT cells. TEM examination of the HEI-OC1 cells incubated for 4 h with NPs of 5 nm diameter did not reveal the presence of NPs within the cells. Moreover, only rare vacuoles were found as relevant ultrastructural changes (not shown). After 24 h incubation, the AgNPs were found both in small endosomes—proving that they entered the cells by endocytosis—and free in the cytoplasm and especially in the nucleus (Figure 6(a)). As in the case of HaCaT cells, the 5 nm AgNPs were still aggregated in clusters inside the HEI-OC1 cells, facilitating their identification. The cells also contained cytoplasmic vacuoles (Figure 6(a)) and autophagosomes (not shown). A number of examined cells were apoptotic, and cellular debris—membranes having attached AgNPs—were also found (not shown). The cells incubated for 4 h with the 25 nm AgNPs showed similar ultrastructural aspects as those previously presented, and also no AgNPs were found in the cells (not shown). After 24 h incubation, the 25 nm AgNPs were found in endosomes (not shown), more frequently aggregated next to the plasma membrane, and also in the proximity of the nucleus (Figure 6(b)). In rare cases, the AgNPs were observed inside the lysosomes (inset of

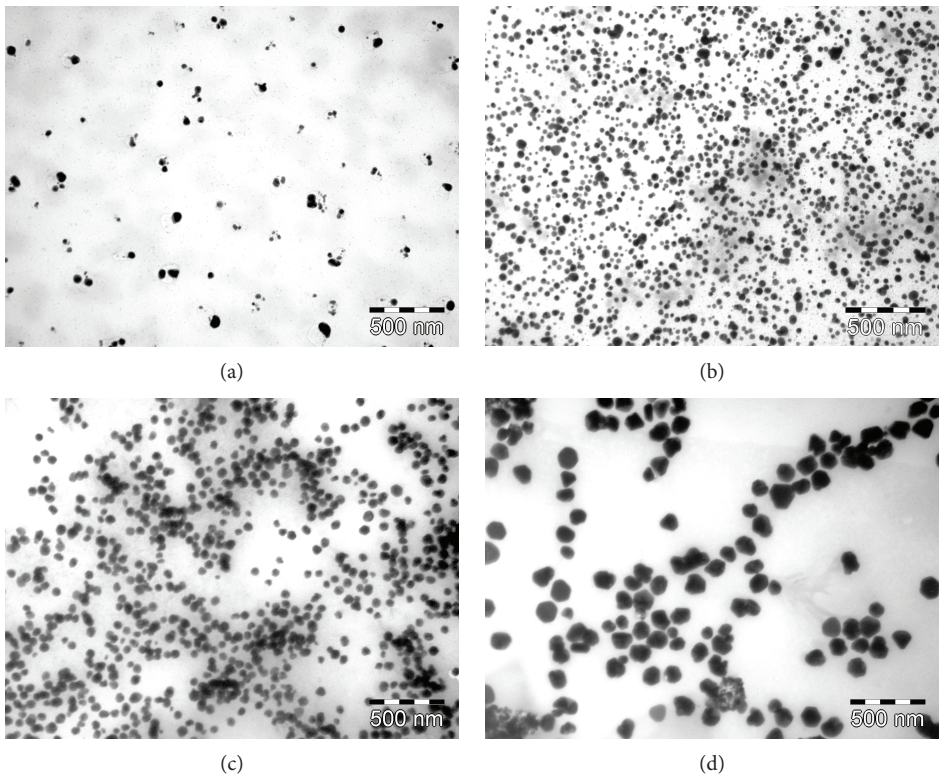

Figure 2: TEM images of AgNPs with diameters of 5 nm (a), 25 nm (b), 50 nm (c), and 110 nm (d).

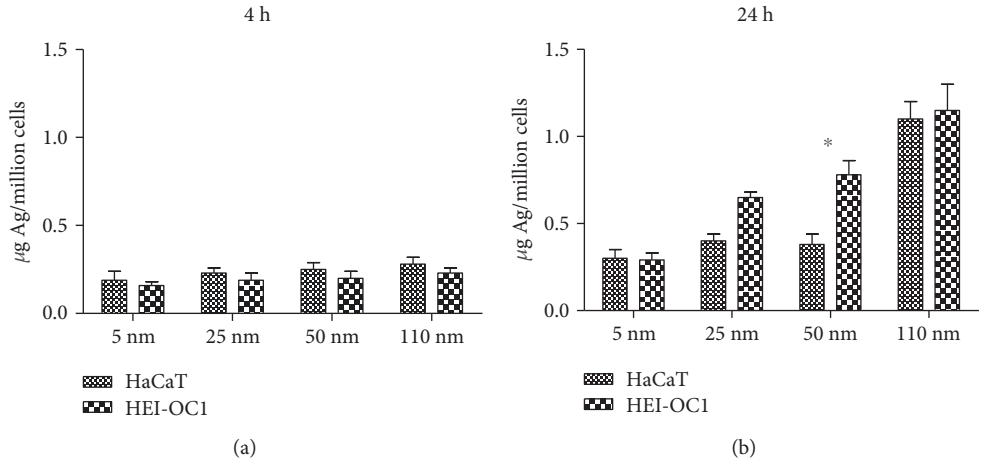

Figure 3: Intracellular silver concentration increased proportionally with the incubation time. After 24 h incubation, the AgNP uptake was more important in HEI-OC1 cells compared to HaCaT, significantly for the 50 nm NPs ($p < 0.1$, two-way ANOVA, Bonferroni posttest). $^{*}p < 0.05$.

Figure 6(b)). These cells presented rare vacuoles within the cytoplasm (Figure 6(b)), and autophagosomes (not shown), and some dead cells were also found (not shown). Consecutive to the 4 h incubation of HEI-OC1 cells with the 50 nm AgNPs, the NPs were found packed in endosomes or as compact groups in contact with the cytoplasm (not shown). Many cells with extensive cytoplasmic vacuolation as well as dead cells were observed (not shown). The 24 h incubation with the 50 nm AgNPs resulted in higher amounts of NPs captured in the cells grouped in different regions of the cytoplasm (Figure 6(c)) and inside the lysosomes (inset of (Figure 6(c)) and endosomes (not shown).

Some cells contained rarefied cytoplasm and numerous vacuoles, while others were dead (not shown). After 4 h incubation of the HEI-OC1 cells with the 110 nm AgNPs, we could not find NPs on the examined sections, but many cells exhibited cytoplasmic vacuolation with heterogeneous content, and some cells were dead (not shown). During the 24 h incubation, the 110 nm AgNPs were found inside the endosomes (Figure 6(d)), others were found as clusters in

Table 2: The treatment of HaCaT and HEI-OC1 cells with AgNPs of four sizes resulted in intracellular concentrations of atomic silver proportional with the NP sizes (after 24 h incubation).

AgNP size	Intracellular Ag concentration (μg/million cells) HaCaT	HEI-OC1
5 nm	0.30 ± 0.05	0.29 ± 0.04
25 nm	0.40 ± 0.04	0.65 ± 0.03
50 nm	0.43 ± 1.1	0.78 ± 0.08
110 nm	1.1 ± 0.8	1.15 ± 0.7

contact with the cytoplasm (upper right inset of Figure 6(d)), and others were found in the lysosomes (lower left inset of Figure 6(d)). There are other ultrastructural features of HEI-OC1 cells treated with AgNPs that are worth mentioning, including the presence in some cells of swollen mitochondria, extensive cytoplasmic vacuolation, and an important number of dead cells, some of them still containing NPs (not shown).

3.4. Cytotoxicity. On both cell lines, AgNPs reduced viability proportionally with their concentration. Viability was also directly proportional with the NP size: the most cytotoxic are the 5 nm NPs, followed by the 25 nm NPs, 50 nm NPs, and 110 nm NPs. The 110 nm NPs were the least toxic on HaCaT cells (Figure 7(a)) as well as on HEI-OC1 cells (Figure 7(b)).

The toxicity of the nanoparticles was also cell line dependent, with the HEI-OC1 cells being more affected by the treatment than the HaCaT cells. IC50, the concentration of AgNPs which reduced viability with 50%, was significantly lower ($p < 0.001$, two-way ANOVA) for all sizes of AgNPs in HEI-OC1 cells (Figure 8).

3.5. Generation of Reactive Oxygen Species (ROS). Treatment with all four sizes of AgNPs resulted in a modulation in the production of ROS compared to control cells in both cell lines. The highest amount of ROS was generated after 2 h exposure. The production of ROS was also proportional with the concentration of the NPs (Figure 9).

Despite being treated with concentrations 10-fold lower than HaCaT cells, HEI-OC1 cells reacted with a significantly stronger ROS production compared to HaCaT cells. The response of the cells to the treatment with AgNPs also depended on the size of the NPs, and the highest amount of ROS was generated in HEI-OC1 cells by the 5 nm AgNPs. It was followed by the largest diameter NPs, the 110 nm NPs, with the 25 nm and 50 nm NPs having a significantly lower effect. HaCaT cells had a completely different response: only the highest concentration of the 50 nm AgNPs generated a significant increase of ROS.

3.6. Comet Assay (Genotoxicity). A 2 h incubation time led to a slight increase of the lesion score (LS) in the treated HaCaT cells compared to the controls, especially for the 5 nm (1.53x increase) and 110 nm (1.7x increase) NPs, although the differences were not significant. In the HEI-OC1 cells, after 2 h incubation, for the 5 nm NPs the increase was 3.77x, followed by the 25 nm (2.44x), 110 nm (2.24x), and 50 nm (2.1x) NPs (Table 3). After 4 h incubation with AgNPs, more important DNA lesions occurred in both cell lines, with the cochlear cells being again more sensitive compared to the keratinocytes. This difference was significant for the 5 nm NPs ($p < 0.1$, two-way ANOVA, Bonferroni posttest) (Figure 10).

4. Discussion

Nanomedicine represents a key player in modern medicine, offering complex systems for targeted drug delivery, new therapies, *in vivo* imaging, etc. As revolutionary treatments of inner ear disorders or for imaging and diagnosis of inner ear conditions, a number of factors, like genes and neurotrophins, have been delivered to the inner ear using NPs as carriers [18]. Currently, AgNPs are among the most preferred antimicrobial nanomaterials used to inhibit the unwanted growth of bacterial biofilms in medical catheters, prostheses, heart valves, etc. It can also represent an attractive alternative to antibiotherapy in the treatment of otitis media. An important aspect is whether these particles can reach the inner ear and whether they are cleared from these structures or remain and accumulate in there. Following transtympanic administration, NPs can pass through the round and oval windows and enter the inner ear [19].

Several studies have shown that the toxicity of nanoparticles is mainly dependent on the particle size. The present study is aimed at assessing the effects of AgNPs as a function of their size on HEI-OC1 cochlear cells compared to the effects of the same NPs on HaCaT cells. We used four sizes of commercially available PVP-coated silver nanoparticles. The uptake of the AgNPs in HEI-OC1 cells and HaCaT cells was evaluated by atomic absorption spectroscopy which showed the intracellular concentration of atomic silver and by TEM which showed the presence of the NPs inside the cells, their localization within the cells, and their effects on the cellular structures. The size-dependent internalization of nanoparticles was demonstrated in a large number of studies being, in general, the highest for 40–50 nm particles [20, 21]. Other factors influencing the uptake of NPs in mammalian cells are considered to be the surface coatings of the particles. However, in a study by Gliga et al., no difference in toxicity between citrate- and PVP-coated 10 nm AgNPs was found, suggesting that the size rather than the capping agent was the property that triggered toxicity [22].

The intracellular silver concentration after treatment with the same concentration of AgNPs of four sizes was proportional with the particle size: the highest silver concentration was found in HEI-OC1 cells after treatment with the 110 nm AgNPs, followed by treatment with the 50 nm AgNPs and 25 nm AgNPs, with the lowest Ag concentration achieved after treatment with the 5 nm AgNPs. Also the Ag concentration was cell type dependent, being higher in the HEI-OC1 cells after 24 h incubation compared to HaCaT cells. Our results showed that the intracellular silver concentration was not correlated with the cytotoxicity of the NPs:

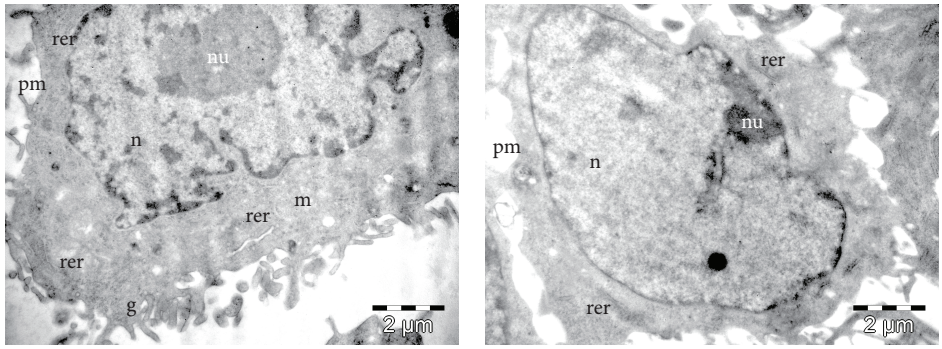

(a) (b)

Figure 4: TEM images of control cells from the two cell lines. (a) Control HaCaT cell with a normal ultrastructure showing a large indented nucleus (n) with a prominent nucleolus (nu), many cell organelles and glycogen granules (g) in the cytoplasm, and a high number of extensions of the plasma membrane (pm). (b) Normal ultrastructure of a cell of the HEI-OC1 line with a large oval nucleus (n) with nucleolus (nu), few profiles of rough endoplasmic reticulum (rer) in the cytoplasm, and a low number of extracellular extensions of the plasma membrane (pm).

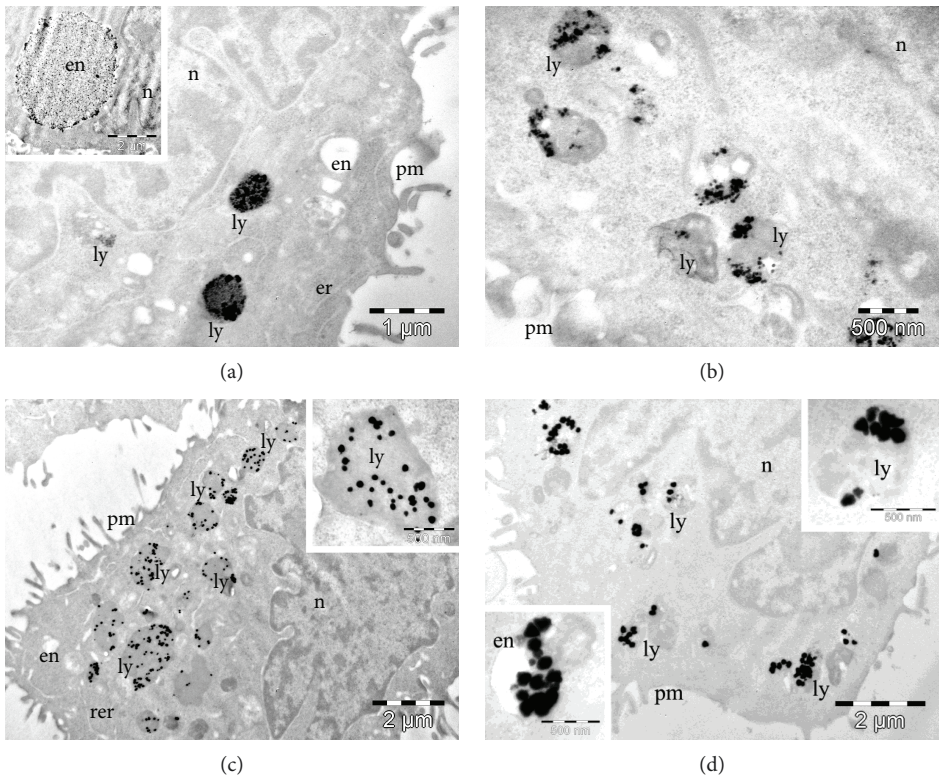

(a) (b)

(c) (d)

Figure 5: Ultrastructure of HaCaT cells incubated for 24 h with the AgNPs with diameters of 5 nm (a), 25 nm (b), 50 nm (c), and 110 nm (d). All types of NPs were captured by the cells, but the NPs of 50 nm were observed with the highest number on our sections (c). The AgNPs were identified in the endosomes (en)—sometimes of large diameters, such as in the case of incubation with NPs of 5 nm (a), as clusters in contact with the cytoplasm, and inside lysosomes (ly). The HaCaT cells incubated with all types of AgNPs had a lower number of plasma membrane (pm) extensions. n—nucleus, rer—endoplasmic reticulum.

the most cytotoxic were the smallest (5 nm) NPs, followed by the 25 nm, 50 nm, and the 110 nm NPs. Thus, high cytotoxicity is not the direct result of silver uptake, a result which was obtained by other studies, as well [22]. The high cytotoxicity of small-sized NPs could be the result of the release of Ag ions in the cell medium, which is significantly higher for the small AgNPs having a larger total surface area and increased particle number for the same mass/volume dose [22]. Other reports showed also that the release of Ag is directly related to the total surface area of the particles as well as the composition of the experimental media [23]. Liu et al. found that 5 nm AgNPs were more toxic than 20 and 50 nm AgNPs in four different tumoral cell lines (A549, HepG2, MCF-7, and SGC-7901) [24].

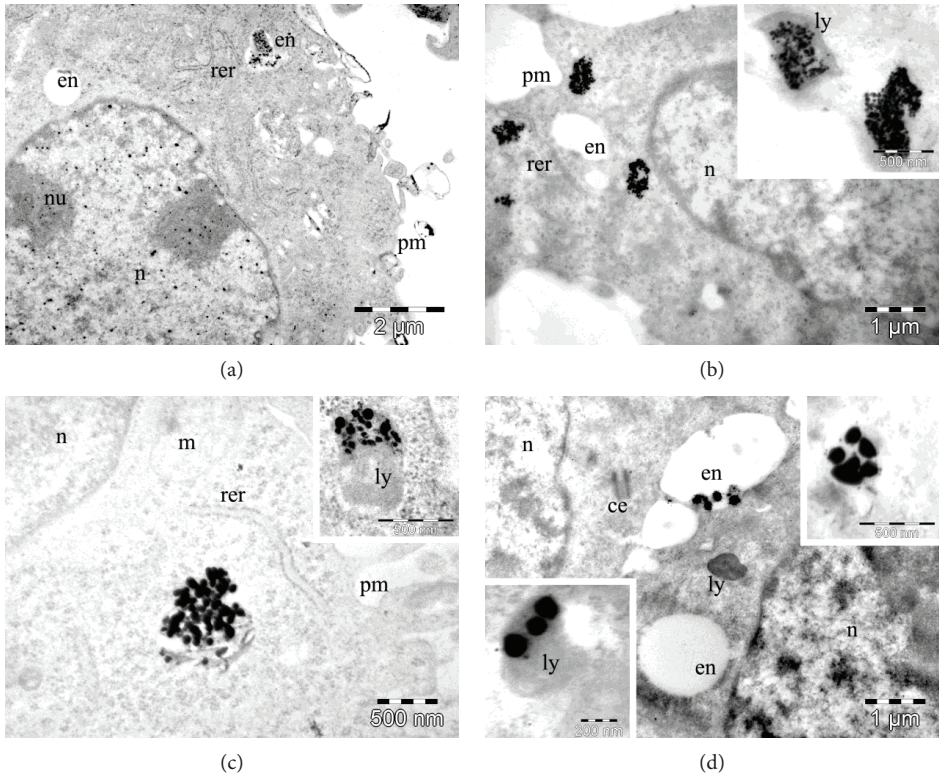

Figure 6: Ultrastructure of HEI-OC1 cells incubated for 24 h with the AgNPs with diameters of 5 nm (a), 25 nm (b), 50 nm (c), and 110 nm (d). The AgNPs are visible as clusters in the endosomes (en) and in the cytoplasm, both next to the plasma membrane (pm) and nucleus (n). The 5 nm AgNPs are also visible inside the nucleus (n). In the lysosomes (ly), the smaller NPs were observed as clusters (a, b) while the larger NPs were relatively dispersed (c, d). ce—centriole, nu—nucleolus, rer—rough endoplasmic reticulum.

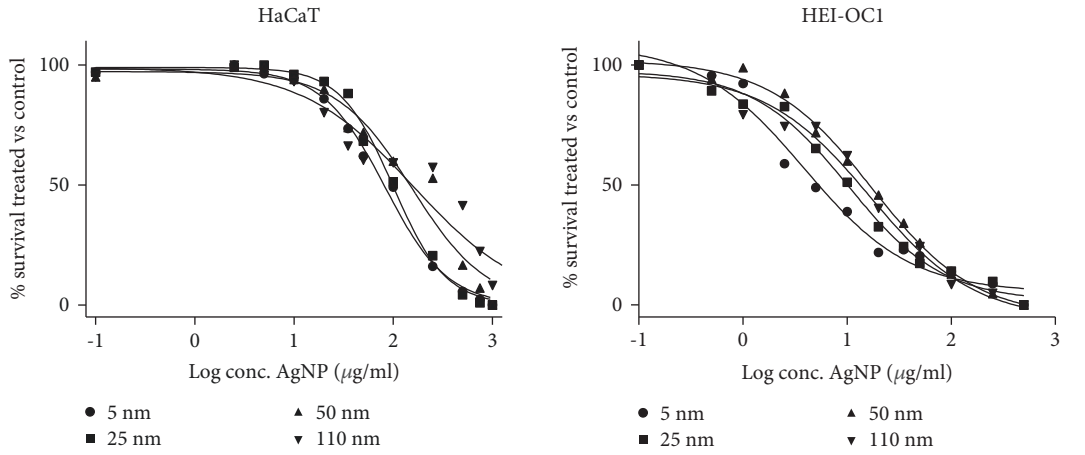

	5 nm	25 nm	50 nm	110 nm
IC50	82.61	99.60	154.4	158.9

(a)

	5 nm	25 nm	50 nm	110 nm
IC50	3.880	10.26	17.50	16.60

(b)

Figure 7: The viability of both cell lines decreased proportionally with the concentration of AgNPs. The toxicity was also size dependent for the AgNPs, with the 5 nm NPs being the most toxic, followed by the 25 nm, 50 nm, and 110 nm NPs in both HaCaT (a) and HEI-OC1 (b) cell lines.

Toxicity was also dependent on the cell line. The viability of HEI-OC1 cells was significantly lower than that of HaCaT cells for the same size and concentration of AgNPs, with the 10-fold difference being important. The cell-type dependent cytotoxicity of NPs was reported in other papers as well: after treatment with silica NPs, THP-1 macrophages were the

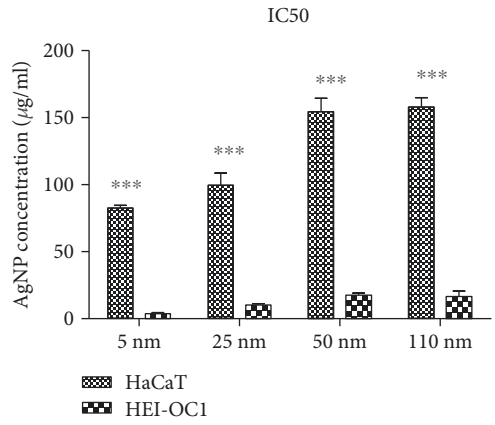

Figure 8: IC50 for the four sizes of AgNPs was significantly higher in HaCaT cells as compared to HEI-OC1 cells, meaning significantly lower toxicity for this cell line compared to the cochlear cells ($p < 0.001$, two-way ANOVA, Bonferroni posttest).

most sensitive cells, followed by A549 cells and HaCaT cells which were the most tolerant. The different behaviour may be explained by different physiological functions and differences in cellular uptake [25]. Studying 23 types of NPs in ten different cell lines, Kroll et al. also reported differences in the sensitivity of the cell lines [26].

Dissolution is an indispensable factor when the toxicity of metal-containing NPs is considered, and this might be the key factor for the high toxicity of the 5 nm AgNPs. This issue is rather complex, since the effect of dissolved Ag ions is associated with other nanospecific factors, as demonstrated by Kim et al. who showed that the toxicity of AgNPs was higher than an equal mass of Ag ions *in vitro* [27].

Recently, Wang et al. showed that citrate- and PVP-coated 20 nm AgNPs induced more cellular toxicity than larger particles (110 nm) and that the citrate-coated 20 nm AgNPs generated acute neutrophilic inflammation in the lungs of exposed mice to a much higher extent when compared to larger ones [28].

In our experiments, the TEM images showed that all AgNPs were uptaken by both types of cells. While after 4 h incubation, only the 5 nm NPs were visualized in the HaCaT cells, after 24 h incubation all sizes of NPs could be observed in both types of cells. Their localization was generally in endosomes, close to the cellular membrane, indicating that they entered the cell via endocytosis, but they were also dispersed in the cytosol or captured in lysosomes. In HEI-OC1 cells, the 5 and 25 nm particles were observed also in the nucleus, where they could have affected the DNA and cell division and thus explaining the higher genotoxicity and cell death. The HEI-OC1 cells showed more ultrastructural changes indicating cellular damage: apoptosis, cellular fragments, and autophagosomes. The intracellular trajectory of NPs is considered to depend on the internalization pathways: they usually enter the early endosomes, they then continue to the late endosomes, and they are finally stored and destroyed by lysosomes [29]. In a study conducted on mammalian kidney cells, AgNPs were localized in membrane-bound structures like lysosomes and early endosomes. The intravesicular localization of AgNPs indicates an uptake through clathrin- or caveolin-mediated endocytosis [30]. The ability of NPs for free diffusion through nuclear pore complexes is associated with their small size which was also the case in our experiments [31].

We next evaluated the mechanisms underlying the effects of different sizes of AgNPs on the two cell lines. We found that after treatment with the AgNPs, there was an increase in ROS production in both types of cells, the most important being recorded after 2 h incubation. The cochlear cells reacted with a more important ROS production, and again the different sizes of AgNPs produced different quantities of ROS. The most potent ROS producers were again the 5 nm NPs. Oxidative damage, caused either by extracellular or by internalized NPs, has been considered by most of the authors studying this issue as the reason for the NP toxicity [32]. High levels of ROS were induced in various mammalian cells especially by AgNPs of less than 20 nm in diameter [24], thus the potential of NPs to induce ROS may be related to their surface area. The majority of the studies indicate an increase in ROS and oxidative stress as a result of AgNP treatment. However, this has been challenged in some studies where no increase in ROS was seen [33]. This may be due to different experimental conditions or due to problems detecting the actual levels of ROS with H2DCFDA, the main dye that was used to detect ROS. The production of intracellular ROS induced by AgNPs most probably lead to DNA damage as several researchers concluded [34, 35].

To evaluate the potential DNA damaging effect of the AgNPs of different sizes, we performed a comet assay after treating both cell lines with AgNPs in the same concentration, for 2 h and 4 h, respectively. We found that DNA damage was also dependent on the NP size and on the cell type. HEI-OC1 cells showed again the most important DNA lesions compared to the HaCaT cells. Lesion scores increased with the exposure time. The 5 nm nanoparticles were the most genotoxic in both cell lines. An explanation could be their ability to enter the nucleus where they induce local ROS which target and damage the DNA. When BEAS-2B cells were treated with a group with noncytotoxic concentrations of AgNPs (10 μg/ml), no significant increase in the percentage of DNA in the comet tail was observed after 4 h exposure to any of the AgNPs. However, a statistically significant increase in overall DNA damage was observed after 24 h for all AgNPs, independent of their size and coating [22]. A comet assay performed in Jurkat Clone E6-1 and THP-1 cells treated with different sizes of AgNPs resulted in DNA lesions inversely correlated with AgNP size, the smaller NPs being more genotoxic. By exposing HaCaT cells to 10 mM or 50 mM nanosilver (in Ag atoms) and with incubation times of 30 min, 4 h, 8 h, and 24 h, a time-dependent increase of direct and oxidative DNA damages was observed [36].

Thus, we can conclude that after AgNPs enter the cells through diffusion or endocytosis, they can cause mitochondrial dysfunction and generation of ROS which will further damage proteins and nucleic acids, inhibiting cell proliferation. Interaction of nanosilver with DNA also leads to cell cycle arrest at the G2/M phase. Park et al. have found that

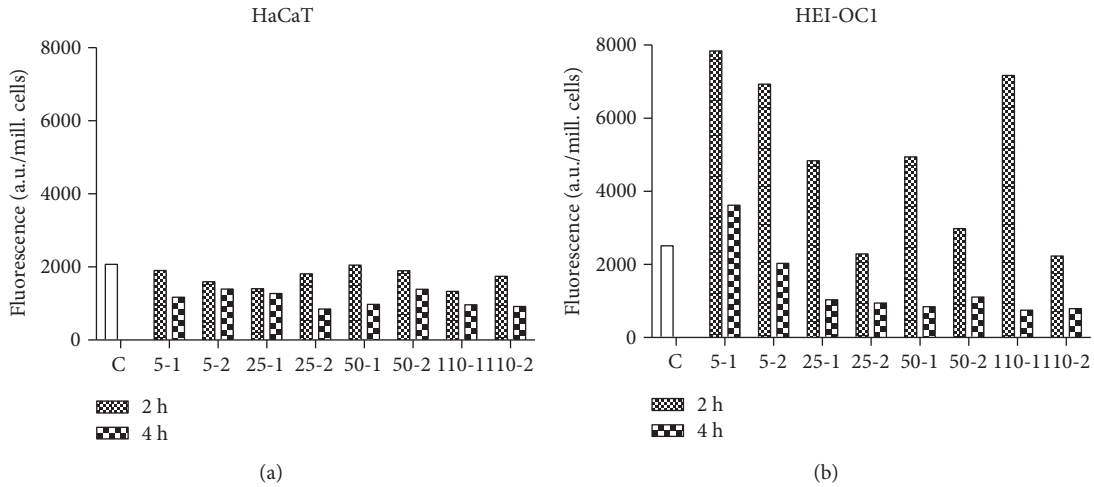

Figure 9: Concentration and size-dependent production of ROS in HaCaT (a) and HEI-OC1 (b) cells. The cells were treated with the AgNPs in 2 concentrations: HaCaT cells with 100 μg/ml (1) and 50 μg/ml (2) and HEI-OC1 cells with 10 μg/ml (1) and 5 μg/ml (2). C—control cells, without AgNPs.

Table 3: AgNPs induced DNA lesion size dependently: the 5 nm NPs induced the most important DNA lesions in both cell lines, followed by the 25 nm, 50 nm, and 110 nm NPs.

Lesion score treated cells vs. control				
AgNP	HaCaT		HEI-OC1	
	2 h	4 h	2 h	4 h
5 nm	↑ 1.53x	↑ 1.98x	↑ 3.77x	↑ 4.07x
25 nm	↑ 1.18x	↑ 1.45x	↑ 2.44x	↑ 2.7x
50 nm	↑ 1.19x	↑ 1.38x	↑2.1x	↑2.62x
110 nm	↑ 1.7x	→	↑2.24x	↑2.39x

↑-fold increase; →-no change.

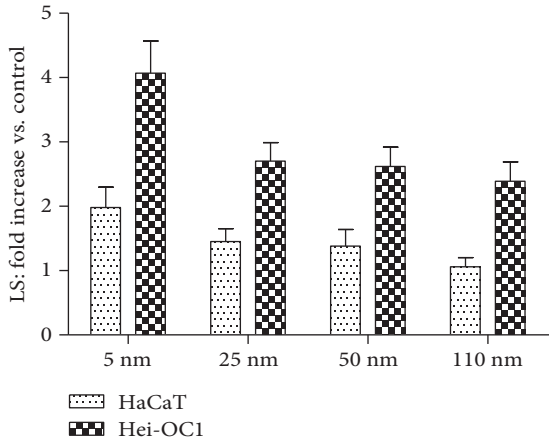

Figure 10: The DNA lesion scores (comet assay) after 4 h exposure to AgNPs were significantly higher in HEI-OC1 cells compared to HaCaT, for all the sizes of the NPs, the difference being significant for the 5 nm NPs ($p < 0.1$, two-way ANOVA, Bonferroni posttest). In both cell lines, the most significant DNA lesions were induced by the 5 nm NPs, followed by the 25 nm, 50 nm, and 110 nm NPs.

nanosilver induces G1 arrest and completely blocks the S phase, therefore inducing apoptosis [37]. The mechanism by which AgNPs exert their effects is probably the result of both Ag ions and the nanoform. Due to surface oxidation, other surface reactions, and dissolution of nanosilver in a biological or environmental medium, silver ions are slowly released. It must be considered that both contribute to the toxicity observed. It is also important to consider some secondary products of nanosilver, such as particles bound to proteins and DNA, for their contribution to toxicity [38].

The release of Ag ions inside cells from nanosilver that entered in its nanoparticle form has been sometimes referred to as the "Trojan horse" effect. Nanosilver itself, and not just the released Ag ions, affect the cellular processes. In addition, silver may be taken up and localized in the cell differently depending on whether it is in its nanoparticle or ionic form, resulting in specific nanoparticle effects.

In general, nanosilver in reasonable doses has many beneficial effects and applications, especially in its antibacterial, antiviral, antifungal, anticancer, and wound healing functions; at the same time, it does not cause adverse effects. As with any compound, high enough doses will induce toxicity, especially in *in vitro* situations [39].

5. Conclusions

Our results show that HEI-OC1 cochlear cells are very sensitive to cytotoxic as well as genotoxic effects of small-sized silver nanoparticles. A strong ROS production in these cells as a response to AgNPs seems to be the main mechanism involved in their sensitivity. Although very attractive, the perspective of using AgNPs in the treatment of otitis media should be regarded with caution and potential treatments of this condition must be carefully tailored.

Data Availability

The imaging and graphical representation data used to support the findings of this study are included within the article.

Conflicts of Interest

The authors declare that they have no conflict of interests.

Acknowledgments

This work was supported the Executive Agency for Higher Education, Research, Development, and Innovation Funding, Romania (grant numbers PN-III-P2-2.1-PED-2016-1857 and 250PED/2017).

References

[1] M. Luntz, N. Yehudai, M. Haifler, G. Sigal, and T. Most, "Risk factors for sensorineural hearing loss in chronic otitis media," *Acta Oto-Laryngologica*, vol. 133, no. 11, pp. 1173–1180, 2013.

[2] B. E. Mostafa, A. G. Shafik, A. M. N. El Makhzangy, H. Taha, and H. M. A. Mageed, "Evaluation of vestibular function in patients with chronic suppurative otitis media," *ORL*, vol. 75, no. 6, pp. 357–360, 2013.

[3] C. T. Nguyen, S. R. Robinson, W. Jung, M. A. Novak, S. A. Boppart, and J. B. Allen, "Investigation of bacterial biofilm in the human middle ear using optical coherence tomography and acoustic measurements," *Hearing Research*, vol. 301, pp. 193–200, 2013.

[4] F. V. Semenov and K. M. Fidarova, "The treatment of the patients presenting with chronic inflammation of the trepanation cavity with a preparation containing silver nanoparticles following sanitation surgery of the open type," *Vestnik Otorinolaringologii*, vol. 6, pp. 117–119, 2012.

[5] M. Xing, L. Ge, M. Wang, Q. Li, X. Li, and J. Ouyang, "Nanosilver particles in medical applications: synthesis, performance, and toxicity," *International Journal of Nanomedicine*, vol. 9, pp. 2399–2407, 2014.

[6] A. Jemec, A. Kahru, A. Potthoff et al., "An interlaboratory comparison of nanosilver characterisation and hazard identification: harmonising techniques for high quality data," *Environment International*, vol. 87, pp. 20–32, 2016.

[7] J. Zou, M. Hannula, S. Misra et al., "Micro CT visualization of silver nanoparticles in the middle and inner ear of rat and transportation pathway after transtympanic injection," *Journal of Nanobiotechnology*, vol. 13, no. 1, p. 5, 2015.

[8] S. H. Shin, M. K. Ye, H. S. Kim, and H. S. Kang, "The effects of nano-silver on the proliferation and cytokine expression by peripheral blood mononuclear cells," *International Immunopharmacology*, vol. 7, no. 13, pp. 1813–1818, 2007.

[9] S. Park, Y. K. Lee, M. Jung et al., "Cellular toxicity of various inhalable metal nanoparticles on human alveolar epithelial cells," *Inhalation Toxicology*, vol. 19, Supplement 1, pp. 59–65, 2008.

[10] S. M. Hussain, A. K. Javorina, A. M. Schrand, H. M. Duhart, S. F. Ali, and J. J. Schlager, "The interaction of manganese nanoparticles with PC-12 cells induces dopamine depletion," *Toxicological Sciences*, vol. 92, no. 2, pp. 456–463, 2006.

[11] S. Arora, J. Jain, J. M. Rajwade, and K. M. Paknikar, "Cellular responses induced by silver nanoparticles: in vitro studies," *Toxicology Letters*, vol. 179, no. 2, pp. 93–100, 2008.

[12] S. Arora, J. Jain, J. M. Rajwade, and K. M. Paknikar, "Interactions of silver nanoparticles with primary mouse fibroblasts and liver cells," *Toxicology and Applied Pharmacology*, vol. 236, no. 3, pp. 310–318, 2009.

[13] S. Moaddab, H. Ahari, D. Shahbazzadeh et al., "Toxicity study of nanosilver (nanocid) on osteoblast cancer cell line," *International Nano Letters*, vol. 1, pp. 11–16, 2011.

[14] S. W. P. Wijnhoven, W. J. G. M. Peijnenburg, C. A. Herberts et al., "Nano-silver – a review of available data and knowledge gaps in human and environmental risk assessment," *Nanotoxicology*, vol. 3, no. 2, pp. 109–138, 2009.

[15] A. Manke, L. Wang, and Y. Rojanasakul, "Mechanisms of nanoparticle-induced oxidative stress and toxicity," *BioMed Research International*, vol. 2013, Article ID 942916, 15 pages, 2013.

[16] L. Zapór, "Effects of silver nanoparticles of different sizes on cytotoxicity and oxygen metabolism disorders in both reproductive and respiratory system cells," *Archives of Environmental Protection*, vol. 42, no. 4, pp. 32–47, 2016.

[17] P. Virag, I. Brie, I. D. Postescu et al., "Comparative study of two evaluation methods for the genotoxic effects of environmental heavy metals on normal cells," *Toxicology and Industrial Health*, vol. 25, no. 4-5, pp. 253–258, 2009.

[18] J. Zou, I. Pyykkö, and J. Hyttinen, "Inner ear barriers to nanomedicine-augmented drug delivery and imaging," *Journal of Otology*, vol. 11, no. 4, pp. 165–177, 2016.

[19] H. Zhou, X. Ma, Y. Liu et al., "Linear polyethylenimine-plasmid DNA nanoparticles are ototoxic to the cultured sensory epithelium of neonatal mice," *Molecular Medicine Reports*, vol. 11, no. 6, pp. 4381–4388, 2015.

[20] R. R. Arvizo, S. Bhattacharyya, R. A. Kudgus, K. Giri, R. Bhattacharya, and P. Mukherjee, "Intrinsic therapeutic applications of noble metal nanoparticles: past, present and future," *Chemical Society Reviews*, vol. 41, no. 7, pp. 2943–2970, 2012.

[21] B. D. Chithrani and W. C. W. Chan, "Elucidating the mechanism of cellular uptake and removal of protein-coated gold nanoparticles of different sizes and shapes," *Nano Letters*, vol. 7, no. 6, pp. 1542–1550, 2007.

[22] A. R. Gliga, S. Skoglund, I. Odnevall Wallinder, B. Fadeel, and H. L. Karlsson, "Size-dependent cytotoxicity of silver nanoparticles in human lung cells: the role of cellular uptake, agglomeration and Ag release," *Particle and Fibre Toxicology*, vol. 11, no. 1, p. 11, 2014.

[23] J. Liu, D. A. Sonshine, S. Shervani, and R. H. Hurt, "Controlled release of biologically active silver from nanosilver surfaces," *ACS Nano*, vol. 4, no. 11, pp. 6903–6913, 2010.

[24] W. Liu, Y. Wu, C. Wang et al., "Impact of silver nanoparticles on human cells: effect of particle size," *Nanotoxicology*, vol. 4, no. 3, pp. 319–330, 2010.

[25] I. L. Hsiao, A. M. Gramatke, R. Joksimovic, M. Sokolowski, M. Gradzielski, and A. Haase, "Size and cell type dependent uptake of silica nanoparticles," *Journal of Nanomedicine & Nanotechnology*, vol. 5, no. 6, 2014.

[26] A. Kroll, C. Dierker, C. Rommel et al., "Cytotoxicity screening of 23 engineered nanomaterials using a test matrix of ten cell lines and three different assays," *Particle and Fibre Toxicology*, vol. 8, no. 1, p. 9, 2011.

[27] S. Kim, J. E. Choi, J. Choi et al., "Oxidative stress-dependent toxicity of silver nanoparticles in human hepatoma cells," *Toxicology In Vitro*, vol. 23, no. 6, pp. 1076–1084, 2009.

[28] X. Wang, Z. Ji, C. H. Chang et al., "Use of coated silver nanoparticles to understand the relationship of particle dissolution and bioavailability to cell and lung toxicological potential," *Small*, vol. 10, no. 2, pp. 385–398, 2013.

[29] I. Pyykkö, J. Zou, Y. Zhang, W. Zhang, H. Feng, and P. Kinnunen, "Nanoparticle based inner ear therapy," *World Journal of Otorhinolaryngology*, vol. 3, no. 4, pp. 114–133, 2013.

[30] M. Milić, G. Leitinger, I. Pavičić et al., "Cellular uptake and toxicity effects of silver nanoparticles in mammalian kidney cells," *Journal of Applied Toxicology*, vol. 35, no. 6, pp. 581–592, 2015.

[31] P. V. AshaRani, M. P. Hande, and S. Valiyaveettil, "Anti-proliferative activity of silver nanoparticles," *BMC Cell Biology*, vol. 10, no. 1, p. 65, 2009.

[32] A. Nel, T. Xia, L. Mädler, and N. Li, "Toxic potential of materials at the nanolevel," *Science*, vol. 311, no. 5761, pp. 622–627, 2006.

[33] Y. Chen, Z. Wang, M. Xu et al., "Nanosilver incurs an adaptive shunt of energy metabolism mode to glycolysis in tumor and nontumor cells," *ACS Nano*, vol. 8, no. 6, pp. 5813–5825, 2014.

[34] Z. Wang, N. Li, J. Zhao, J. C. White, P. Qu, and B. Xing, "CuO nanoparticle interaction with human epithelial cells: cellular uptake, location, export, and genotoxicity," *Chemical Research in Toxicology*, vol. 25, no. 7, pp. 1512–1521, 2012.

[35] M. V. D. Z. Park, A. M. Neigh, J. P. Vermeulen et al., "The effect of particle size on the cytotoxicity, inflammation, developmental toxicity and genotoxicity of silver nanoparticles," *Biomaterials*, vol. 32, no. 36, pp. 9810–9817, 2011.

[36] K. S. Butler, D. J. Peeler, B. J. Casey, B. J. Dair, and R. K. Elespuru, "Silver nanoparticles: correlating nanoparticle size and cellular uptake with genotoxicity," *Mutagenesis*, vol. 30, no. 4, pp. 577–591, 2015.

[37] E. J. Park, J. Yi, Y. Kim, K. Choi, and K. Park, "Silver nanoparticles induce cytotoxicity by a Trojan-horse type mechanism," *Toxicology In Vitro*, vol. 24, no. 3, pp. 872–878, 2010.

[38] D. McShan, P. C. Ray, and H. Yu, "Molecular toxicity mechanism of nanosilver," *Journal of Food and Drug Analysis*, vol. 22, no. 1, pp. 116–127, 2014.

[39] S. Cameron, F. Hosseinian, and W. Willmore, "A current overview of the biological and cellular effects of nanosilver," *International Journal of Molecular Sciences*, vol. 19, no. 7, p. 2030, 2018.